Hearing Research 321 (2015) 52–64

Contents lists available at ScienceDirect

Hearing Research

journal homepage: www.elsevier.com/locate/heares

Research paper

Deletion of *Shank1* has minimal effects on the molecular composition and function of glutamatergic afferent postsynapses in the mouse inner ear

Jeremy P. Braude [a], Sarath Vijayakumar [b], Katherine Baumgarner [a], Rebecca Laurine [a], Timothy A. Jones [b], Sherri M. Jones [b], Sonja J. Pyott [a, *]

[a] University of North Carolina Wilmington, Department of Biology and Marine Biology, 601 South College Road, Wilmington, NC 28403, USA
[b] University of Nebraska Lincoln, Department of Special Education and Communication Disorders, 304B Barkley Memorial Center, Lincoln, NE 68583-0738, USA

ARTICLE INFO

Article history:
Received 9 October 2014
Received in revised form
24 December 2014
Accepted 13 January 2015
Available online 28 January 2015

ABSTRACT

Shank proteins (1–3) are considered the master organizers of glutamatergic postsynaptic densities in the central nervous system, and the genetic deletion of either Shank1, 2, or 3 results in altered composition, form, and strength of glutamatergic postsynapses. To investigate the contribution of Shank proteins to glutamatergic afferent synapses of the inner ear and especially cochlea, we used immunofluorescence and quantitative real time PCR to determine the expression of Shank1, 2, and 3 in the cochlea. Because we found evidence for expression of Shank1 but not 2 and 3, we investigated the morphology, composition, and function of afferent postsynaptic densities from defined tonotopic regions in the cochlea of Shank1$^{-/-}$ mice. Using immunofluorescence, we identified subtle changes in the morphology and composition (but not number and localization) of cochlear afferent postsynaptic densities at the lower frequency region (8 kHz) in Shank1$^{-/-}$ mice compared to Shank1$^{+/+}$ littermates. However, we detected no differences in auditory brainstem responses at matching or higher frequencies. We also identified Shank1 in the vestibular afferent postsynaptic densities, but detected no differences in vestibular sensory evoked potentials in Shank1$^{-/-}$ mice compared to Shank1$^{+/+}$ littermates. This work suggests that Shank proteins play a different role in the development and maintenance of glutamatergic afferent synapses in the inner ear compared to the central nervous system.

1. Introduction

Excitatory glutamatergic transmission in the cochlea occurs between the sensory inner hair cells (IHCs) and their afferent fibers and relies on specialized multi-molecular, pre- and postsynaptic structures. Presynaptic ribbons are electron-dense structures that tether glutamate-filled synaptic vesicles and enable multi-vesicular release (see recent review by Safieddine et al., 2012). Glutamate activates postsynaptic AMPA receptors (Glowatzki and Fuchs, 2002) that are part of postsynaptic densities (PSDs) on the afferent dendrites (Meyer et al., 2009). Although recent work has contributed greatly to our understanding of the molecular components that shape release from the hair cell ribbons, we know considerably less about how the molecular organization of the PSD shapes afferent responses.

PSDs of the cochlear afferent dendrites are morphologically (Nouvian et al., 2006) and molecularly (Davies et al., 2001) similar to glutamatergic PSDs found in the central nervous system (CNS; reviewed in Sheng and Hoogenraad, 2007): they are electron dense, oppose presynaptic structures, and contain similar proteins, including a variety of glutamate receptor subtypes and canonical postsynaptic density (PSD) proteins. These PSD proteins include signaling and scaffolding proteins that have long been appreciated to shape AMPA receptor expression (including localization, recruitment, and recycling) and, thereby, the diversity of responses

Abbreviations: IHC, inner hair cell; AMPAR, α-amino-3-hydroxy-5-methyl-4-isoxazolepropionic acid receptor; PSD, postsynaptic density; CNS, central nervous system; ABR, auditory brainstem response; VsEPs, vestibular evoked potentials; CTBP2, C-terminal-binding protein 2; DIC, differential interference contrast; GKAP, guanylate kinase-associated protein

* Corresponding author. Current address: University Medical Center Groningen, Department of Otorhinolaryngology, PO Box 30.001, 9700 RB Groningen, The Netherlands. Tel.: +31 050 361 4653.
E-mail address: s.pyott@umcg.nl (S.J. Pyott).

http://dx.doi.org/10.1016/j.heares.2015.01.008
0378-5955/

seen in glutamatergic synapses of the CNS (reviewed in Sager et al., 2009). Like central glutamatergic synapses, across mammals, auditory afferents, even those contacted by the same hair cell, can display enormous diversity in their responses, including differences in thresholds and spontaneous firing rates (Liberman, 1982; el Barbary, 1991; Tsuji and Liberman, 1997; Taberner and Liberman, 2005). Recent work identified differences in AMPA receptor expression that may contribute to differences in auditory nerve thresholds and spontaneous firing rates (Liberman et al., 2011). Moreover, auditory sensitivity *in vivo* has been shown to be regulated by reversible changes in surface AMPAR expression in the cochlea (Chen et al., 2007). These previous findings suggest that, as in the CNS, differences in PSD composition shape glutamatergic responses in the cochlea.

Of the variety of proteins comprising the PSD, Shank proteins (1–3) are found in nearly all glutamatergic synapses in the CNS and are considered the "master" organizers of the PSD (reviewed in Sheng and Kim, 2000). Shank proteins constitute a significant part of the overall protein content of the PSD and, via various protein–protein interaction and multimerization domains, link AMPA and other glutamate receptor subtypes to the cytoskeleton. In the CNS, shank proteins are also involved in the dynamic structural and molecular reorganization of dendritic spines (Sala et al., 2001). Knockout mice for Shank1 (Hung et al., 2008), 2 (Schmeisser et al., 2012) and 3 (Peca et al., 2011; Schmeisser et al., 2012) are viable and their molecular and behavioral phenotypes have been examined. Compared to wild type mice, Shank1 knockout mice display altered molecular composition of postsynaptic density proteins, reduced number and size of dendritic spines and thinner PSDs, and decreased AMPA receptor-mediated synaptic strength (Hung et al., 2008). Since comparable synaptopathies are observed in Shank2$^{-/-}$ and Shank3$^{-/-}$ mice, there is likely only partial redundancy in the function of Shank family members.

These observations from the CNS coupled with the recent identification by immunofluorescence of Shank1 in the afferent PSDs of the developing cochlea (Huang et al., 2012), led us to hypothesize that Shank proteins are also essential components of cochlear afferent PSDs and that the absence of Shank proteins would disrupt the structural and molecular organization of the PSD and result in auditory deficits. To investigate this hypothesis, we examined the expression of Shank1, 2, and 3 in the cochlear inner ear by both immunofluorescence and quantitative real time PCR (qPCR). Because we identified only Shank1 in the cochlear inner ear, we then examined for changes in afferent synaptic organization and function in Shank1$^{-/-}$ mice, which presumably lack all known Shank isoforms. To our surprise we observed only subtle changes in the morphology and composition of IHC afferent PSDs and no changes in auditory brainstem responses (ABRs) in Shank1$^{-/-}$ mice compared to Shank1$^{+/+}$ littermates. Similarly, there was no observed deficit in the vestibular function of Shank1$^{-/-}$ mice compared to Shank1$^{+/+}$ littermates.

2. Materials and methods

2.1. Animals

All experimental procedures were carried out in accordance with the Institutional Animal Care and Use Committees (IACUCs) at both the University of North Carolina Wilmington and the University of Nebraska Lincoln. C57BL/6 were used for initial experiments (Fig. 1) and were obtained from the The Jackson Laboratory. For all other experiments (Figs. 2-6), 129S4/SvJae Shank1^{tmShng}-heterozygous (Shank1$^{+/-}$) mice were obtained from The Jackson Laboratory. Homozygous wild type (Shank1$^{+/+}$) and knockout (Shank1$^{-/-}$) mice were obtained from crosses of heterozygous (Shank1$^{+/-}$) mouse matings. Genotyping was performed using a protocol described previously (Truett et al., 2000; Silverman et al., 2011). All data were collected from mice aged 4 weeks and from littermates originating from at least three different litters for each experimental condition.

2.2. Immunofluorescence of auditory and vestibular sensory epithelia

Mice were anaesthetized via halothane inhalation before being sacrificed. Auditory and vestibular sensory epithelia were isolated

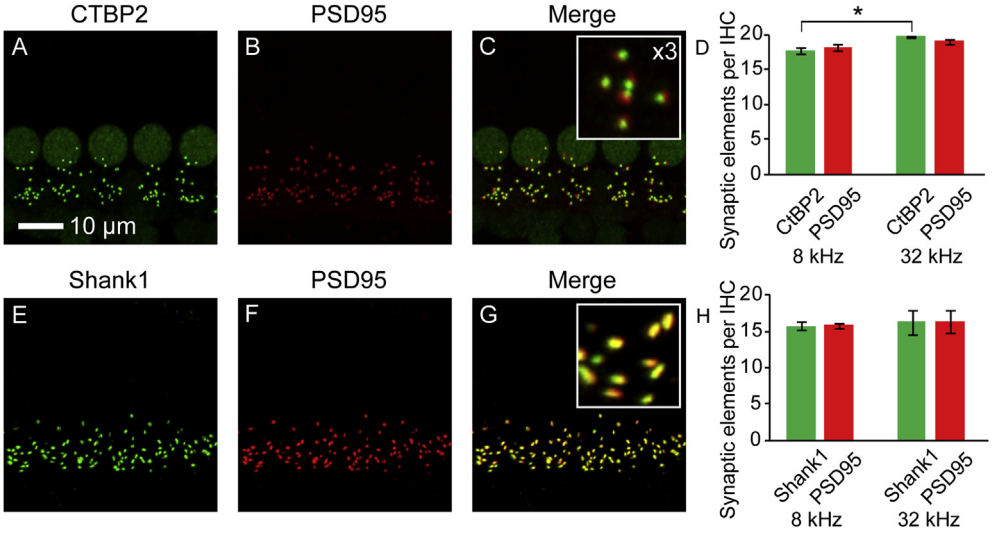

Fig. 1. Shank1 is a component of inner hair cell (IHC) afferent postsynaptic densities (PSD). Organs of Corti from 4 week old mice were immunostained with either a mouse monoclonal IgG1 antibody against CTBP2 (green, A) or rabbit polyclonal antibody against Shank1 (green, E) and a mouse monoclonal IgG2A antibody against PSD95 (red, B,F). Observations of individual samples revealed that almost every presynaptic CTBP2-positive ribbon was juxtaposed to a PSD95-positive PSD and vice versa (C) and that almost every PSD95-positive PSD also expressed Shank1 immunoreactivity and vice versa (G). Images are presented as Z-projections of a stack of confocal micrographs from the 32 kHz region. Mean values (±SEM) of CTBP2-positive presynaptic ribbons (D) or Shank1-positive PSDs (H) and PSD95-positive PSDs across samples are compared at two tonotopic regions (8 and 32 kHz). Statistically significant differences are indicated with an asterisk. (For interpretation of the references to color in this figure legend, the reader is referred to the web version of this article.)

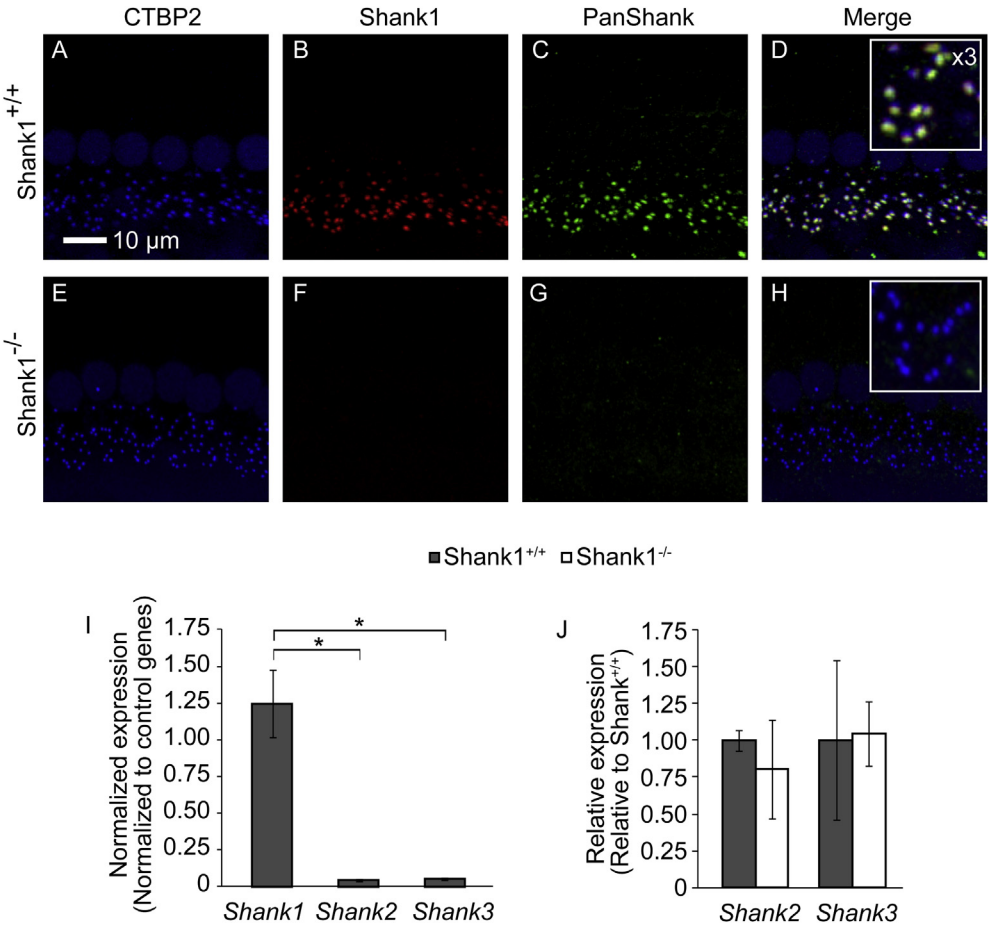

Fig. 2. Shank proteins are not detected in the cochleae of inner hair cell (IHC) afferent postsynaptic densities (PSD) from Shank1$^{-/-}$ mice nor is there compensatory upregulation of *Shank2* or *Shank3* in cochlea from Shank1$^{-/-}$ mice. Organs of Corti from 4 week old Shank1$^{+/+}$ (A–D) and Shank1$^{-/-}$ (E–H) littermate mice were immunostained with a mouse monoclonal IgG1 antibody against CTBP2 (blue, A and E), a rabbit polyclonal antibody against Shank1 (red, B and F) and a goat polyclonal antibody that recognizes all three Shank isoforms (panShank, green, C and G). Colocalized Shank1 and panShank immunoreactivity was observed juxtaposed to CTBP2-positive presynaptic ribbons in Shank1$^{+/+}$ mice (D). Although CTBP2-positive presynaptic ribbons were observed, neither Shank1 nor panShank immunoreactivity was observed in Shank1$^{-/-}$ mice (H). Images are presented as Z-projections of a stack of confocal micrographs from the 16 kHz region. *Shank1-3* transcript expression was investigated in the cochleae of Shank1$^{+/+}$ mice (and presented normalized to control gene expression in Shank1$^{+/+}$ mice, I). *Shank2-3* transcript expression was investigated in Shank1$^{-/-}$ mice (and presented relative to *Shank2* and *Shank3* expression in Shank1$^{+/+}$ mice, J). Two-fold or more greater changes in expression are indicated with asterisks. (For interpretation of the references to color in this figure legend, the reader is referred to the web version of this article.)

and immunostained as described previously (McLean et al., 2009; Schuth et al., 2014). The primary antibodies used in this study are listed in Table 1. Alexa Fluor secondary antibodies (Life Technologies) included: goat anti-mouse IgG1 488; goat anti-mouse IgG2b 488 and 647; goat anti-mouse IgG2a 594 and 647; goat anti-rabbit IgG 488 and 568; donkey anti-goat 488; donkey anti-rabbit 594; and donkey anti-mouse 647.

2.3. Confocal microscopy and image analysis

Micrographs were acquired using an Olympus Fluoview FV1000 confocal microscope 10× air or 60× oil immersion lens under the control of the Olympus Fluoview FV10-ASW 2.1 software (Olympus Corporation). For organs of Corti, tonotopic maps were superimposed on low magnification micrographs of complete organs of Corti in ImageJ (http://www.masseyeandear.org/research/ent/eaton-peabody/epl-histology-resources and Mueller et al., 2005). High magnification confocal micrographs of identified tonotopic regions of the organ of Corti were collected to encompass the entire synaptic pole of the row of IHCs from the 8 kHz and also 32 kHz region. High magnification confocal micrographs of the striolar region of the vestibular sensory epithelium of the utricular macula were similarly collected to encompass the entire synaptic pole of the sensory hair cells. For both the auditory and vestibular sensory epithelia, the step size (optical section thickness) was determined by stepping at half the distance of the theoretical z-axis resolution (the Nyquist sampling frequency). Images were acquired in a 1024 × 1024 raster (x = y = 0.207 µm/pixel) at sub-saturating laser intensities for each channel. Images are presented as z-projections through the collected optical stack. All quantitative image analysis was performed on the raw image stacks, without deconvolution, filtering, or gamma correction.

3D reconstructions were obtained using Imaris 6.4 software (Bitplane Inc.) and used to determine the number and volume of synaptic elements for the two tonotopic regions of organs of Corti. To determine the number of synaptic elements per IHC, the Imaris spot detection function was used to detect immunopuncta corresponding to specific synaptic proteins within a given field of view. This value was then divided by the total number of IHCs within that field of view. IHC counts were obtained from counts of immunofluorescently detected IHC nuclei (for CTBP2 immunolabeling) and/or DIC-imaged IHC bodies (when CTBP2 immunolabeling was not performed). Volumes (µm^3) of immunopuncta corresponding to specific synaptic proteins were calculated from contour surfaces

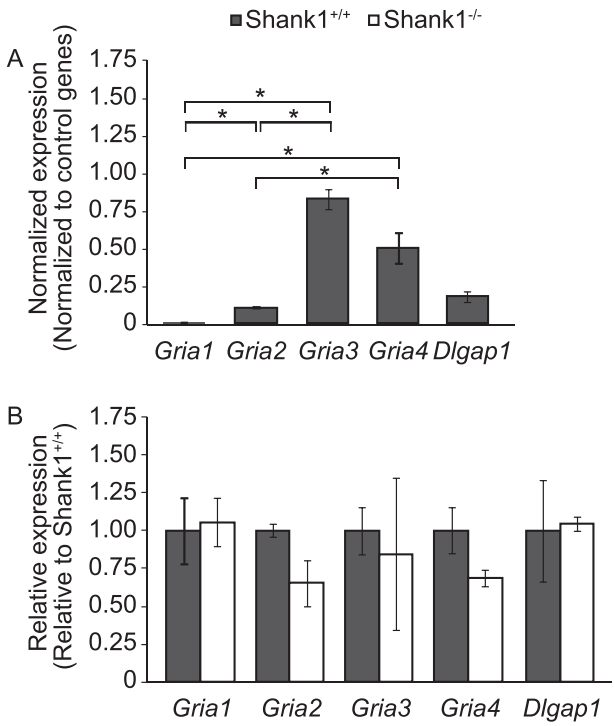

Fig. 3. Cochleae from Shank1$^{-/-}$ mice show minimal changes in transcript abundances for genes encoding GluA1-4 and GKAP. *Gria1-4* and *Dlgap1* transcript expression was investigated in the cochleae of Shank1$^{+/+}$ mice (normalized to control gene expression in Shank1$^{+/+}$ mice, A) and Shank1$^{-/-}$ mice (relative to *Gria1-4* and *Dlgap1* expression in Shank1$^{+/+}$ mice, B). Two-fold or more greater changes in expression are indicated with asterisks.

generated in Imaris using a surface area detail of 0.2 μm. All numerical values were exported for further statistical analyses.

2.4. Primer design, RNA extraction, and quantitative real time PCR (qPCR)

Primers for *Shank1-3*, *Gria1-4*, *Dlgap1*, *Hprt1*, *B2m*, and *Pgk1* were either designed or selected from primer bank (pga.mgh.harvard.edu/primerbank) and are provided in Table 2. Amplicons were selected from exons that are expressed in all known splice variants of the given gene as determined using the UCSC genome browser database (genome.ucsc.edu). Additionally, another *Shank1* primer set was designed to target the amplicon in the deleted region of the gene in Shank1$^{-/-}$ mice. Primer sequences were selected using Primer3 software (frodo.wi.mit.edu), and *in-silico* PCR (UCSC genome browser) was performed to confirm a single PCR product for each primer set. The primers and amplicons were aligned with their mRNA reference sequences from GenBank (www.ncbi.nlm.nih.gov) using Sequencher software (Gene Codes Corporation) to confirm homogeneity in the primer and amplicon sequences.

Organs of Corti and spiral ganglion cell bodies were dissected from Shank1$^{+/+}$ and Shank1$^{-/-}$ mice. A total of four cochlea (both cochleae from two individuals of the same genotype) were pooled for each biological replicate. Three unique biological replicates for each genotype were collected. Dissected samples were immediately placed into ice-cold lysis buffer (RNAqueous®-Micro Kit, Life Technologies), flash frozen in liquid nitrogen, and stored at −80 °C until RNA was extracted. Total RNA was extracted (without DNase treatment) using the RNAqueous®-Micro Kit (Life Technologies) according to the manufacturer's instructions. RNA quality was determined using the 2100 Bioanalyzer (Agilent), and RNA quantity was determined using the Nanodrop 2000 (Thermo Scientific). cDNA synthesis was performed using the iScript™ cDNA Synthsis Kit (BioRad) according to the manufacturer's instructions. qPCR was performed using the SsoAdvanced™ SYBR® Green Supermix (Bio-Rad) reagent and MyiQ™ Single-Color Real-Time PCR Detection System (BioRad). The cycling protocol included an initial denaturing step at 95 °C for 3 min followed by 40 cycles of 95 °C for 10 s, 60 °C for 30 s and 72 °C for 30 s. Biological replicates and control samples were run as triplicates. Primer specificity to single amplicons was confirmed by examining melting curves and identifying single peaks. qPCR was also performed on the negative controls from the reverse transcription reaction to confirm that amplicons originated from the cDNA pool. Amplicon identity was subsequently verified by DNA sequencing (Macrogen, USA). Quantification of gene expression was performed using the relative standard curve method (as described in Larionov et al., 2005), with target gene expression normalized against the geometric mean of the three control genes. *Shank1-3*, *Gria1-4*, and *Dlgap1* transcript expression in Shank1$^{+/+}$ mice is presented as the normalized transcript expression of each gene (that is, normalized to the expression of the control genes *Hprt1*, *B2m*, and *Pgk1* in Shank1$^{+/+}$ mice). To examine relative changes in gene expression in Shank1$^{-/-}$ compared to Shank1$^{+/+}$ mice, *Shank2-3*, *Gria1-4*, and *Dlgap1* transcript expression is presented as the normalized expression (that is, normalized to the expression of the control genes in Shank1$^{-/-}$ mice) relative to the normalized expression of *Shank2-3*, *Gria1-4*, and *Dlgap1* in Shank1$^{+/+}$ mice. Thus, relative expression values close to 1 would suggest little to no relative differences in transcript expression between genotypes or, more specifically, little to no up or down regulation in Shank1$^{-/-}$ compared to Shank1$^{+/+}$ mice. Importantly, no significant variations in control gene expression were observed between or within genotypes.

2.5. Functional assessment of auditory and vestibular function

Auditory brainstem responses (ABRs) and vestibular sensory evoked potentials (VsEPs) were measured for Shank1$^{-/-}$ and Shank1$^{+/+}$ littermates using methods similar to those described previously (Jones et al., 1999, 2004; Mock et al., 2011). Mice were anaesthetized via a ketamine (18 mg/mL) and xylazine (2 mg/mL) solution (5–7 μL/g body weight) injected intraperitoneally. Core body temperature was maintained at 37 °C using a homeothermic heating pad (FHC, Inc.).

For ABRS, pure tone burst stimuli were generated and controlled using National Instruments data acquisition system and custom software. Tone bursts at 8, 16, and 32 kHz had 1.0 ms rise and fall times with 1.0 ms plateau (3 ms total duration). Stimuli for ABR testing were calibrated using a Bruel & Kjaar ¼ inch microphone and Nexus amplifier. Stimuli were calibrated in dB peSPL and were presented via high frequency transducers (ED1 driver, EC1 speakers, Tucker–Davis Technologies) coupled at the left ear via a modified commercial ear tip (ER 10D-T03, Etymotic Research, Inc.). Auditory stimuli were presented at a rate of 17 stimuli/s. ABR intensity series were collected by reducing the stimulus in 10 dB steps at higher stimulus levels and 5 dB steps closer to threshold. P1–N1 amplitudes and P1 latencies are presented as the input–output (I/O) function slopes of the amplitude and latency growth function curves (that is, amplitude and latency as a function of stimulus intensity) as described previously (Burkard et al., 1990; Jones and Jones, 1999).

DPOAE stimuli were generated and controlled using TDT System III (RX6, PA5 modules) and SigGen/BioSig software. Pure tone frequencies (f1, f2, f2/f1 ratio = 1.25), at equal levels (L1 = L2 = 60 dB SPL), 150 ms duration, were generated by RX6 multifunction

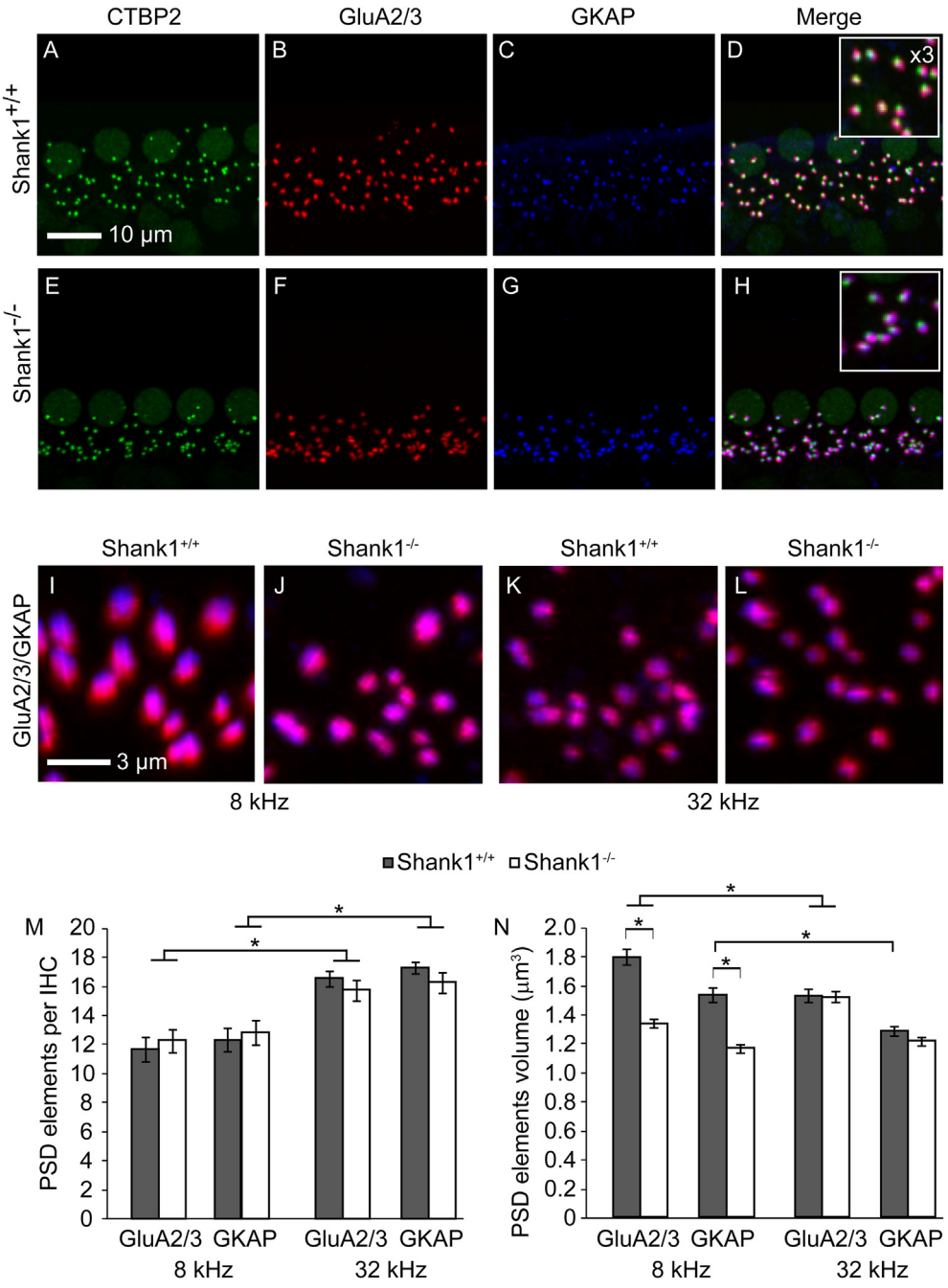

Fig. 4. Inner hair cell (IHC) afferent postsynaptic densities (PSDs) from Shank1$^{-/-}$ mice show subtle changes in their morphology and composition. Organs of Corti from 4 week old Shank1$^{+/+}$ (A-D,I,K) and Shank1$^{-/-}$ (E-H,J,L) littermate mice were immunostained with a mouse monoclonal IgG1 antibody against CTBP2 (green, A and E), a rabbit polyclonal antibody against GluA2/3 (red, B and F,I-L), and a mouse monoclonal IgG2B antibody against GKAP (blue, C and G,I-L). Colocalized GluA2/3 and GKAP immunoreactivity was observed juxtaposed to CTBP2-positive presynaptic ribbons in both Shank1$^{+/+}$ (D) and Shank1$^{-/-}$ mice (H). Images are presented as Z-projections through a stack of confocal micrographs from the 32 kHz region (A–H) or as 3D reconstructions comparing the 8 and 32 kHz region (I–L) from Shank1$^{+/+}$ and Shank1$^{-/-}$ mice. Mean values (±SEM) of GluA2/3-positive and GKAP-positive immunopuncta per hair cell (M) and mean values (±SEM) of GluA2/3-positive and GKAP-positive immunopuncta volumes (N) for each genotype are compared at two tonotopic regions (8 and 32 kHz). Statistically significant differences are indicated with an asterisk. (For interpretation of the references to color in this figure legend, the reader is referred to the web version of this article.)

processor, attenuated through PA5 programmable attenuators and routed through separate drivers to mix acoustically in the ear canal via the same eartip used for ABR testing. Primary stimulus frequencies were such that the geometric mean [GM = $(f1 \times f2)^{0.5}$] frequencies ranged from 6.0 to 48.5 kHz. Ear canal sound pressure levels were recorded with a low noise probe microphone (ER 10B+, Etymotic Research Inc., Elk Grove Village, IL). The microphone output was amplified (10×) and routed to RX6 multifunction processor for sampling at 100 kHz and Fast Fourier transforms (FFT) of the averaged responses. The amplitudes of f1, f2, and the cubic (2f1−f2) distortion product were measured from the FFT waveform. The corresponding noise floor was determined from sound levels in the eleven frequency bins above and below the 2f1−f2 frequency bin.

For VsEPs, stimuli were delivered by securing the mouse head using a noninvasive head clip to a mechanical shaker (Model ET-

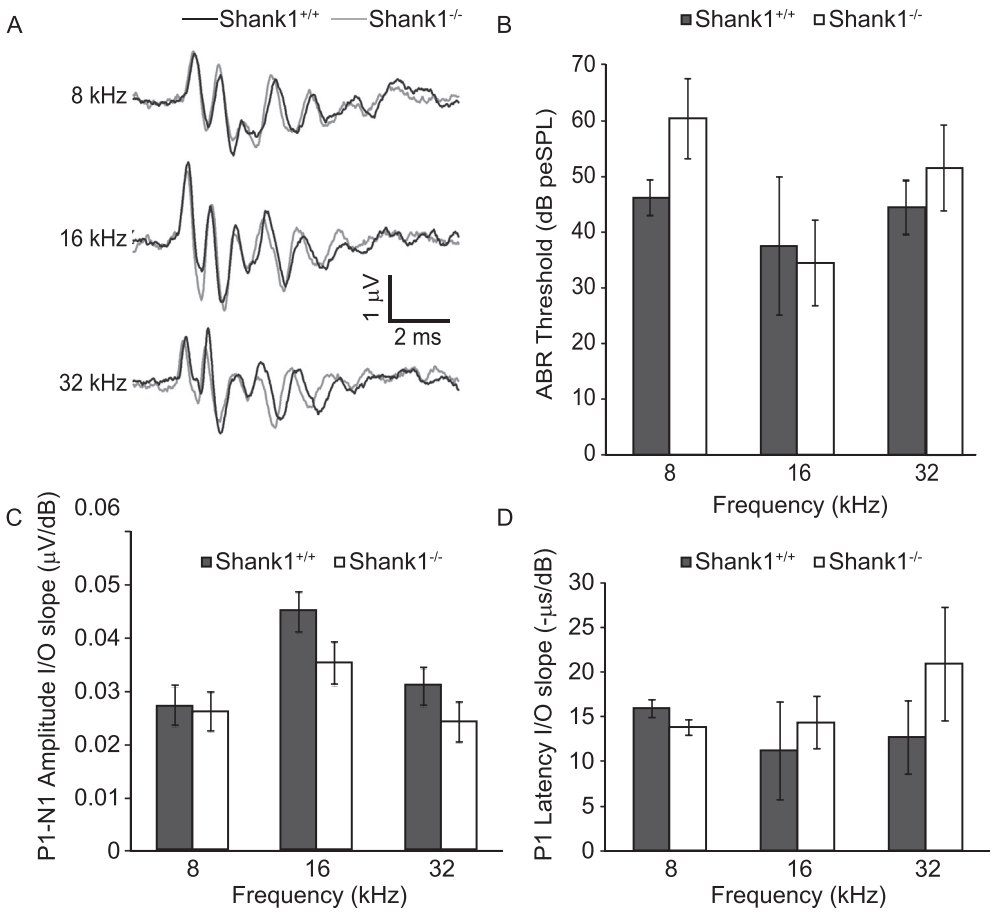

Fig. 5. Auditory brainstem responses are comparable in Shank1$^{+/+}$ and Shank1$^{-/-}$ mice. ABR raw traces (A), thresholds (B), P1–N1 amplitude (I/O) slopes (C), and P1 latency I/O slopes (D) are compared between genotypes across frequencies.

132-203, Labworks Inc.) Linear acceleration pulses (17 pulses/s, 2 ms duration) ranging in amplitude from +6 to −18 dB re: 1.0 g/ms (where 1 g = 9.8 m/s^2) adjusted in 3 dB steps were presented to the head in the naso-occipital axis. Subcutaneous needle electrodes were placed posterior to the right pinna and at the right hip for inverting and ground electrodes, respectively. Stainless-steel wire placed subcutaneously at the nuchal crest served as the non-inverting electrode. Electroencephelographic activity was amplified (200,000×), filtered (300–3000 Hz), and digitized (1024 points at 10 μs/point). 256 primary responses were averaged and replicated for each VsEP waveform. VsEP intensity series were collected with and without acoustic masking (50–50,000 Hz forward masker at 90 dB SPL) beginning with the maximum stimulus intensity (i.e., +6 dB re: 1.0 g/ms) and then descending in 3 dB steps until no response was visible.

2.6. Statistical analyses

Except for qPCR data, in which values are presented as mean ± SDM, all other group results are reported as the mean ± SEM. Mean values for synaptic elements per IHC were calculated across individuals of a given genotype and frequency (i.e., from the average of the synaptic elements per IHC calculated for an individual). Mean values for the volumes of synaptic elements were calculated from pooled values for a given genotype and frequency. Statistical analyses were performed using GraphPad Prism 4 (GraphPad Inc). Ordinary one-way ANOVA followed by a Tukey's multiple comparison test was used to determine statistically significant differences between the indicated groups. P values <0.05 were considered statistically significantly different (and are indicated with asterisks in the figures). For qPCR data, transcript abundances differing more than two-fold were considered statistically significantly different (and are indicated with asterisks in the figures).

3. Results

3.1. Shank1, but not Shank 2 and 3, is expressed in inner hair cell afferent PSDs

We investigated the localization of central glutamatergic scaffolding proteins in the mouse organ of Corti using immunofluorescent labeling and confocal microscopy at two tonotopically distinct regions, 8 kHz and 32 kHz. By immunostaining for C-terminal binding protein 2 (CTBP2, green, Fig. 1A), an established marker for hair cell ribbons (Khimich et al., 2005), using a mouse monoclonal (IgG1) antibody, we compared the localization of presynaptic active sites to that of PSD95 (red, Fig. 1B), an established marker of glutamatergic PSDs in the CNS and also identified in the cochlea (Davies et al., 2001), using a mouse monoclonal IgG2A antibody (Fig. 1A–C). Observations of individual samples revealed that almost every presynaptic CTBP2-positive ribbon was juxtaposed to a PSD95-positive PSD and vice versa (Fig. 1C). To obtain values of synaptic elements per IHC, the total number of IHCs was determined by counting the total number of CTBP2-positive nuclei as well as total number of DIC-imaged IHCs. Values for the total

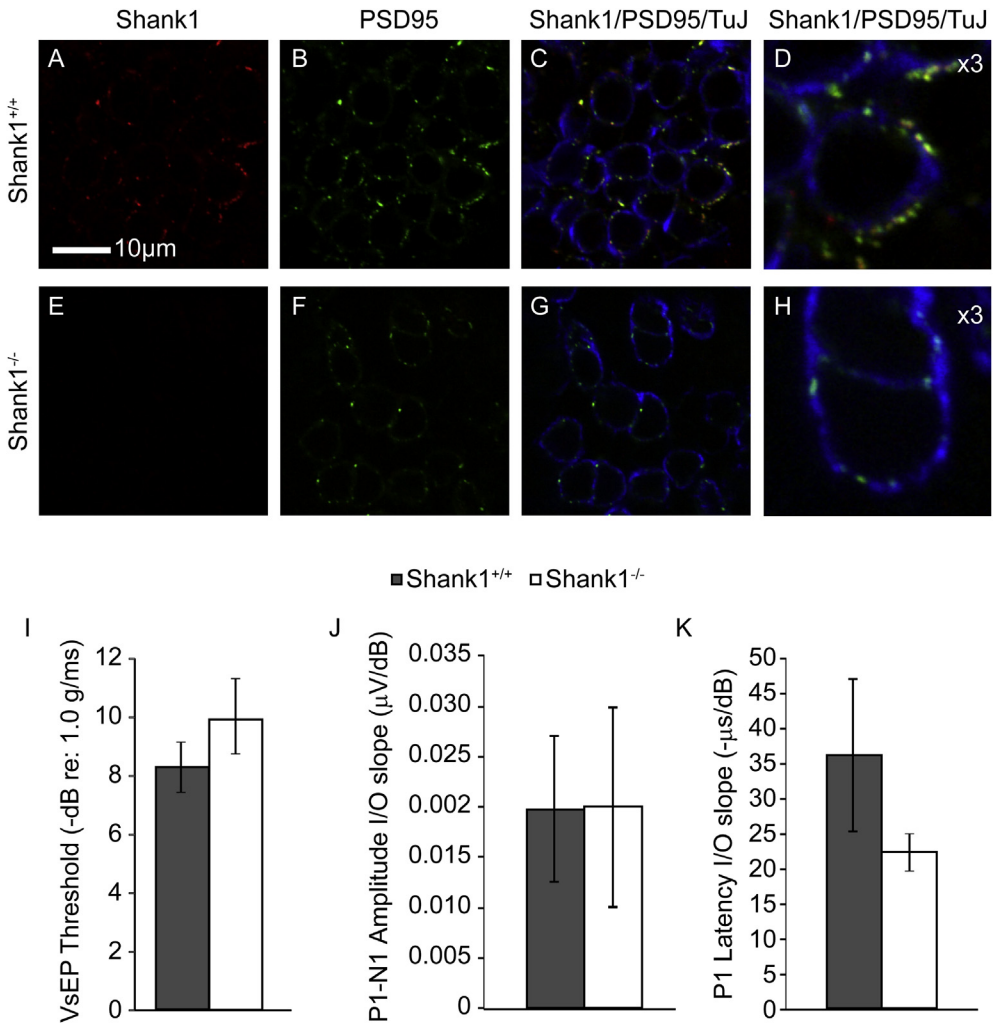

Fig. 6. Vestibular function is comparable in Shank1$^{+/+}$ and Shank1$^{-/-}$ mice. The vestibular sensory epithelia of the utricular maculae was isolated from 4 week old Shank1$^{+/+}$ (A–D) and Shank1$^{-/-}$ (E–H) mice and immunostained with a rabbit polyclonal antibody against Shank1 (red, A and E), a mouse monoclonal IgG2A antibody against PSD95 (green, B and F), and a mouse monoclonal antibody against tubulin J (TuJ, blue, C and G). Shank1 immunoreactivity was colocalized to PSD95-positive PSDs observed in TuJ-positive calyx and bouton afferent terminals in Shank1$^{+/+}$ mice (D). In contrast, no Shank1 immunoreactivity was observed in PSD95-positive PSDs in Shank1$^{-/-}$ mice (H). Images are presented as a single optical section from the striolar region. Vestibular evoked potentials (VsEPs) showed comparable thresholds (I), P1–N1 amplitude (I/O) slopes (J) and P1 latency I/O slopes (K) between genotypes. (For interpretation of the references to color in this figure legend, the reader is referred to the web version of this article.)

number of IHCs were identical regardless of methodology. Across samples, mean values for synaptic elements per IHC were comparable for both CTBP2-positive and PSD95-positive immunopuncta (Fig. 1D). At 8 kHz, there was a mean of 17.7 ± 0.5 CTBP2-positive ribbons (n = 2163 immunopuncta) and 18.2 ± 0.5 PSD95-positive PSDs (n = 2220 immunopuncta) per IHC (n = 122 IHCs from 5 individuals). At 32 kHz, there was a mean of 19.7 ± 0.1 CTBP2-positive ribbons (n = 2504 immunpuncta) and 19.0 ± 0.4 PSD95-positive PSDs (n = 2403) per IHC (n = 127 IHCs from the same 5 individuals; Fig. 1D). There was no significant difference in the number of CTBP2-positive ribbons and PSD95-positive PSDs at either 8 or 32 kHz. However, the difference in CTBP2-positive ribbons at 8 compared to 32 kHz was significantly different (with approximately 2 fewer ribbons per IHC at 8 kHz). Although not investigated specifically in our analyses, these results of statistical analyses suggest that the likelihood of finding PSD95-positive PSDs not juxtaposed to CTBP2-positive ribbons is slightly greater in higher (32 kHz) compared to lower (8 kHz) frequencies. This 1:1 relationship between pre- and postsynaptic elements (at a given frequency) has been reported before in the organ of Corti (Khimich et al., 2005; Liberman et al., 2011). Perhaps due to strain differences, we observed slightly higher numbers of synaptic elements per IHC than previous immunofluorescent quantifications, which reported maximal values of approximately 17 synapses per IHC in the mouse organ of Corti (Meyer et al., 2009; Liberman et al., 2011; Vincent et al., 2014). Importantly, because we also find PSD95-positive PSDs juxtaposed to presynaptic ribbons in a nearly 1:1 relationship, we can conclude that PSD95 is present in all IHC afferent PSDs.

After establishing PSD95 to be a reliable marker of all IHC afferent PSDs, we investigated whether and to what extent Shank1 is present in IHC afferent PSDs (Fig. 1E–H). For these experiments, we performed double immunolabeling experiments using a rabbit polyclonal antibody against Shank1 (green, Fig. 1E) and the mouse monoclonal antibody (IgG2A) against PSD95 (red, Fig. 1F). Shank1 has been previously localized to afferent synapses in the apical organs of Corti isolated from developing (P0, 3, 6, and 12) and adult (P35-42) mice using an antibody different from the one used in this study (Huang et al., 2012). Similar to these previous findings, we observed Shank1 in the IHC-afferent (Fig. 1E) but not OHC-afferent (data not shown) synapses. Observations of individual samples from both tonotopic regions further revealed that almost every PSD95-positive PSD also expressed Shank1 immunoreactivity and

Table 1
Primary antibodies for immunofluorescence.

Target protein(s)	Antibody isotype	Epitope/Immunogen	Accession number	Vendor	Catalog number
CTBP2	Mouse IgG1	aa 361-445 (mouse CtBP2)	Not provided	BD Biosciences	612044
PSD95	Mouse IgG2a	Fusion protein aa 77-299 (human PSD-95)	P78352	Neuromab	75-028
Shank1	Rabbit IgG	SGPIYPGLFDIRSS (Shank1a C-teminus)	Not provided	Neuromics	RA19016
Shank1	Mouse IgG1	Fusion protein amino acids 469-691 (rat Shank1)	Q9WV48	Neuromab	
Shank2	Mouse IgG1	Fusion protein aa 84-309 (rat Shank2)	Q9QX74	Neuromab	75-088
Shank3	Mouse IgG2b	Synthetic peptide aa 840-857 PEKLPGSLRKGIPRTKSV (rat Shank3)	QNJLU4	Neuromab	75-109
panShank	Goat IgG	C-terminus (human Shank1)	Q9Y566	Santa Cruz Biotechnology	sc-23543
GluA2/3	Rabbit IgG	EGYNVYGIESVKI (rat GluR2 C-terminus)	NP_000817	Millipore	AB1506
GKAP	Mouse IgG2b	Fusion protein aa 772-992 (rat GKAP1)	P97836	Neuromab	75–156
TuJ	Mouse IgG1	ESESQGPK (human human class III β-tubulin	NM_00686.2	Millipore	MAB1637

vice versa (Fig. 1G). Thus, across samples, mean values for synaptic elements per DIC-imaged IHC were comparable for both Shank1-positive and PSD95-positive immunopuncta (Fig. 1H). At 8 kHz, there were 15.8 ± 0.6 Shank1-positive PSDs (n = 1586) and 15.8 ± 0.4 PSD95-positive PSDs (n = 1592) immunopuncta per IHC (n = 101 IHCs from 4 individuals). At 32 kHz, there were 16.3 ± 1.7 Shank1-positive PSDs (n = 1653 immunopuncta) and 16.3 ± 1.5 PSD95-positive PSDs (n = 1652 immunopuncta) per IHC (n = 100 IHCs from the same 4 individuals). There were no significant differences between any of the six possible comparisons of synaptic elements per IHC and tonotopic region. Similar patterns of Shank1 immunoreactivity were also observed when we used a mouse monoclonal antibody to Shank1 (data not shown). These findings indicate that Shank1 is a component of IHC afferent PSDs.

To validate the specificity of Shank1 immunoreactivity, we triple immunolabeled organs of Corti isolated from Shank1$^{+/+}$ and Shank1$^{-/-}$ littermate mice with the mouse monoclonal antibody against CTBP2 (blue, Fig. 2A,E), the rabbit polyclonal antibody against Shank1 (red, Fig. 2B,F), and a goat polyclonal antibody that recognizes all three Shank isoforms (panShank, green, Fig. 2C,G). For these experiments, a single tonotopic region (16 kHz) was isolated. As expected, in organs of Corti isolated from Shank1$^{+/+}$ mice, we observed Shank1-positive immunopuntca (Fig. 2B) juxtaposed to CTBP2-positive presynaptic ribbons (Fig. 2A,D). We also observed panShank-positive immunopuncta (Fig. 2C) colocalized with Shank1-positive immunopuncta and juxtaposed to CTBP2-positive ribbons (Fig. 2D). In organs of Corti isolated from Shank1$^{-/-}$ littermate mice, we still observed CTBP2-positive ribbons (Fig. 2E), indicating that afferent presynaptic ribbons are conserved in the absence of Shank1. In contrast, we observed no immunoreactivity for Shank1 (Fig. 2F,H). These findings confirm the specificity of the Shank1 polyclonal antibody. Interestingly, we also observed no immunoreactivity for panShank in organs of Corti isolated from Shank1$^{-/-}$ mice (Fig. 2G,H). The presence of panShank immunoreactivity in the organs of Corti isolated from Shank1$^{+/+}$ mice but not Shank1$^{-/-}$ littermate mice suggest that Shank1 is the only Shank isoform present in IHC afferent PSDs in the mouse organ of Corti. To corroborate this finding, we examined immunoreactivity in organs of Corti from Shank1$^{+/+}$ using mouse monoclonal antibodies specifically recognizing Shank2 and Shank3. We found no immunoreactivity with either of these antibodies (data not shown). Thus, the IHC afferent PSDs in Shank1$^{-/-}$ mice appear to be devoid of all identified Shank isoforms, suggesting that Shank1$^{-/-}$ mice provide an excellent model to examine the contribution of Shank proteins in general to the synaptic organization and function of IHC afferent PSDs.

Table 2
Primers for qPCR.

Gene	Sequence		Amplicon size	UCSC genome locus	PrimerBank ID
Shank 1	Fwd	ATCAGTGCAAGTGAGAGTCCTG	135	Chr7: 51600307–51606371	–
	Rev	GAAAGAAGGCCGGTCATAACT			
Shank1 (exon 14–16)	Fwd	TGCAGAAGAAGGACAGTGAGG	235	chr7: 51597500–51598473	–
	Rev	TGTCGGATCATGTTGACCAC			
Shank 2	Fwd	GGCAAATGTCATTAGTGAGCTAAA	160	Chr7: 151597654–151606503	–
	Rev	GCTCCGTGTACCTGAGACG			
Shank 3	Fwd	ATTCCACGGACCAAATCTGT	106	Chr15: 89374288–89378140	–
	Rev	CTCGACCTTCACGCACTGT			
DLGAP1	Fwd	AAGGTGGCTGCAAGAAGAGA	136	Chr17: 70942651–71006858	–
	Rev	CACTTACGGCCCTCAGGTAG			
GRIA1	Fwd	CAAGTTTTCCCGTTGACACATC	165	chr11: 56999406–57003190	357527404c2
	Rev	CGGCTGTATCCAAGACTCTCTG			
GRIA2	Fwd	ACGACGACTCCCTGGTGTCTA	144	Chr3: 80514712–80526042	–
	Rev	TGCGGAATGCTTCAGTCATC			
GRIA3	Fwd	GTGCAGTTATACAACACCAACCA	113	chrX: 41402854–41402966	163792195c2
	Rev	GAGCAGAAAGCATTAGTCACAGA			
GRIA4	Fwd	TTCCGAGCAGCGTTCAAATAG	154	chr9: 4793837–4795207	164419754c1
	Rev	CAGTCTCAATGTTGTCCACATGA			
HPRT1	Fwd	TGACACTGGTAAAACAATGCA	94	ChrX: 50369532–50373300	–
	Rev	GGTCCTTTTCACCAGCAAGCT			
PGK1	Fwd	ATGTCGCTTTCCAACAAGCTG	164	ChrX: 103382590–103389742	6679291a1
	Rev	GCTCCATTGTCCAAGCAGAAT			
B2M	Fwd	TTCTGGTGCTTGTCTCACTGA	104	Chr2: 121973499–121976670	144227219c1
	Rev	CAGTATGTTCGGCTTCCCATTC			

To further confirm the absence of all Shank isoforms in the organs of Corti from Shank1$^{-/-}$ mice, we examined *Shank1-3* transcript expression in the organs of Corti and spiral ganglion cells (SGCs) isolated from Shank1$^{+/+}$ and Shank1$^{-/-}$ mice using qPCR. Although evidence supports the dendritic localization of Shank transcripts (Boeckers et al., 2004), we also included SGC bodies to ensure transcripts (which are synthesized in the cell bodies) were detected if present. As described in the Methods, *Shank1-3*, *Gria1-4*, *Dlgap1*, *Hprt1*, *B2m*, and *Pgk1* transcript expression in Shank1$^{+/+}$ mice is presented as the normalized transcript expression of each gene (that is, normalized to the expression of the control genes in Shank1$^{+/+}$ mice). In samples from Shank1$^{+/+}$ mice, we found 30-fold greater expression of *Shank1* compared to either *Shank2* or *Shank 3* (Fig. 2I). Relative to control gene expression, we found expression levels in Shank1$^{+/+}$ mice of 1.25 ± 0.23 for *Shank1*, 0.04 ± 0.01 for *Shank2*, and 0.05 ± 0.01 for *Shank3* (Fig. 2I). To examine relative changes in gene expression in Shank1$^{-/-}$ compared to Shank1$^{+/+}$ mice, *Shank2-3*, *Gria1-4*, *Dlgap1*, *Hprt1*, *B2m*, and Pgk1 transcript expression is presented as the normalized expression (that is, normalized to the expression of the control genes in Shank1$^{-/-}$ mice) relative to the normalized expression of *Shank2-3*, *Gria1-4*, *Dlgap1*, *Hprt1*, *B2m*, and *Pgk1* in Shank1$^{+/+}$ mice. Thus, relative expression values close to 1 would suggest little to no relative differences in transcript expression between genotypes. Relative to *Shank2* and *Shank3* expression in Shank1$^{+/+}$ mice, we found expression levels in Shank1$^{-/-}$ mice of 0.80 ± 0.33 for *Shank2* and 1.04 ± 0.22 for *Shank 3*, suggesting no compensatory up or down regulation of *Shank2* or *Shank3* in the cochleae of Shank1$^{-/-}$ mice (Fig. 2J). As expected, very low *Shank1* signal was detected in samples collected from Shank1$^{-/-}$ mice, so relative expression is not plotted in Fig. 2J. Together with our observations of protein expression using immunofluorescence, these findings are consistent with the conclusion that Shank1 is the primary and likely exclusive Shank isoform found in the cochlea and that Shank1$^{-/-}$ mice are, therefore, devoid of all known Shank isoforms.

3.2. The composition of cochlear afferent PSDs is subtly altered in the absence of Shank1

To identify potential changes in the molecular composition of cochlear (and especially IHC) afferent PSDs, which are comprised of a multitude of proteins, resulting from the absence of Shank1, we examined the presence and relative transcript abundance of the genes encoding the four GluA subtypes (*Gria1-4*). We also examined expression of *Dlgap1*, a gene that encodes the protein guanylate kinase-associated protein (GKAP). GKAP binds directly to both Shank and PSD95 and is critical for recruitment and accumulation of Shank and the assembly of PSDs (Sheng and Kim, 2000). In this way, we could assess possible changes in the receptor types mediating cochlear afferent synaptic transmission as well as changes more deeply in the molecular scaffold of the cochlear afferent PSD. Of the four *Gria* transcripts examined, in wildtype Shank1$^{+/+}$ mice (normalized to control gene expression), both *Gria3* and *Gria4* were significantly more abundantly expressed than *Gria2*; *Gria2, 3 and 4* were all significantly more expressed than *Gria1*; and *Gria1* was expressed at very low levels. (Normalized expression values were: *Gria1*: 0.017 ± 0.003; *Gria2*: 0.101 ± 0.003; *Gria3*: 0.822 ± 0.066; and *Gria4*: 0.499 ± 0.100.) These values are highly consistent with previous findings from the rat cochlea: both immunocytochemical localization (Kuriyama et al., 1994; Matsubara et al., 1996) and *in situ* hybridization (Luo et al., 1995) report abundant GluA2/3 (or *Gria2* and *Gria3*) expression and no GluA1 (or *Gria1*) expression. We also detected transcript expression of *Dlgap1* (0.176 ± 0.036). Although there was a decrease in mean values for *Gria2* and *Gria4* relative transcript abundance in Shank1$^{-/-}$ relative to expression of *Gria2* and *Gria4* in Shank1$^{+/+}$ samples across all three biological replicates, no genotypic differences in expression (greater than two-fold) were observed for any of the genes (*Gria1-4* and *Dlgap1*) examined. (Expression values in Shank1$^{-/-}$ mice relative to gene expression in Shank1$^{+/+}$ mice were: *Gria1*: 1.06 ± 0.16; *Gria2*: 0.65 ± 0.15; *Gria3*: 0.85 ± 0.50; *Gria4*: 0.69 ± 0.05; and *Dlgap1*: 1.04 ± 0.04. Again, relative expression values close to 1 would suggest little to no relative differences in transcript expression between genotypes).

To examine for changes in protein expression, and especially AMPAR expression suggested by the changes in transcript abundance, we examined GluA2/3 and also GKAP expression in the IHC afferent PSD of organs of Corti isolated from Shank1$^{+/+}$ and Shank1$^{-/-}$ littermate mice using immunofluorescence as described in the Methods and used previously to quantify relative protein abundances/distributions (Wersinger et al., 2010; Maison et al., 2013). Specifically, we triple immunolabeled organs of Corti with a mouse monoclonal (IgG1) antibody against CTBP2 (green, Fig. 4A,E), a rabbit polyclonal antibody that recognizes both the GluA2 and 3 subtypes (GluA2/3, red, Fig. 4B,F,I-L), and a mouse monoclonal (IgG2B) antibody against GKAP (blue, Fig. 4D,H,I-L). The antibody against GluA2/3 was chosen because it reliably labels the most abundantly expressed GluA in the cochlea (GluA3). Unfortunately, antibodies that reliably detect individual GluA subtypes, especially for GluA2-4, in our hands, have not been identified. In organs of Corti isolated from either Shank1$^{+/+}$ or Shank1$^{-/-}$ mice, we observed CTBP2-positive ribbons juxtaposed to GluA2/3- and GKAP-positive PSDs (Fig. 4D,H). These findings indicated no overt qualitative changes in PSD localization or composition in the absence of Shank1.

To more rigorously examine PSD number and composition, we calculated the number of PSD elements per IHC (Figure 4M) from 3D reconstructions of confocal micrographs spanning the entire afferent synaptic pole from two tonotopic locations (8 kHz and 32 kHz). Mean values are summarized in Table 3. The mean number of GluA2/3- and GKAP-positive PSDs did not vary by genotype at either of the two frequencies. However, there were significantly greater PSD elements (approximately 4 per IHC) at 32 kHz compared to 8 kHz for both genotypes. Tonotopic differences were not observed when examining PSD95-positive PSDS (Fig. 1) and may reflect strain differences: C57BL/6 mice were used to collect the data in Fig. 1 whereas all other data were collected from Shank1$^{+/+}$ and Shank1$^{-/-}$ mice on the 129/SvJae background strain. The bases of these differences were not investigated further. Notwithstanding, these results indicate that the absence of Shank proteins causes no obvious alteration in the number of IHC afferent PSDs and the presence of key PSD proteins in the IHC afferent PSDs across tonotopic ranges.

In addition to characterizing the number of IHC afferent PSDs and the presence of GluA2/3 and GKAP in the IHC afferent PSDs, we also examined the volumes of the GluA2/3 and GKAP immunopuncta from 3D reconstructions to assess differences in their relative protein abundances and/or distribution in the absence of Shank proteins (Fig. 4I–L, N). Methodologically similar quantifications of relative protein abundances/distributions have been used previously (Wersinger et al., 2010; Maison et al., 2013), and relative abundances/distributions determined using immunofluorescence parallel abundances/distribution determined using electrophysiology (Pyott et al., 2004). Mean values of immunopuncta volumes are summarized in Table 4. Between the two genotypes, we found significantly smaller volumes for both GluA2/3 and GKAP immunopuncta at the 8 kHz region in Shank1$^{-/-}$ mice compared to Shank1$^{+/+}$ littermate mice. There were no statistically significant differences in either GluA2/3 or GKAP immunopuncta volumes between genotypes at 32 kHz. Between the two frequencies, GluA2/

Table 3
PSD elements per IHC.

	8 kHz				32 kHz			
	GluA2/3		GKAP		GluA2/3		GKAP	
	Shank1$^{+/+}$ (n = 4)	Shank1$^{-/-}$ (n = 7)	Shank1$^{+/+}$ (n = 4)	Shank1$^{-/-}$ (n = 7)	Shank1$^{+/+}$ (n = 4)	Shank1$^{-/-}$ (n = 7)	Shank1$^{+/+}$ (n = 4)	Shank1$^{-/-}$ (n = 7)
Mean ± SEM	11.7 ± 0.9	12.3 ± 0.8	12.3 ± 0.8	12.8 ± 0.9	16.5 ± 0.5	15.8 ± 0.7	17.3 ± 0.4	16.3 ± 0.7
N (immunopuncta)	1237	2432	1306	2535	1736	2821	1816	2920
N (IHCs)	105	199	105	199	105	180	105	180

3 immunopuncta volumes were significantly larger at 8 kHz compared to 32 kHz in Shank1$^{+/+}$ mice. In contrast, GluA2/3 immunopuncta volumes were significantly smaller at 8 kHz compared to 32 kHz in Shank1$^{-/-}$ mice. Similarly, we observed significantly larger GKAP immunpuncta at 8 kHz compared to 32 kHz in Shank1$^{+/+}$ mice. There was no statistically significant difference in GKAP immunpuncta volumes between frequencies in Shank1$^{-/-}$ mice. These data suggest that the loss of Shank indeed alters the abundance and/or distribution of PSD proteins specifically at lower frequency tonotopic regions.

3.3. Cochlear function is normal in the absence of Shank1

The findings of IHC afferent PSDs of reduced size (GluA2/3 and GKAP immunoreactive volumes) in the 8 but not 32 kHz region of Shank1$^{-/-}$ mice compared to Shank1$^{+/+}$ littermate mice predicts potential low frequency auditory deficits in the Shank1$^{-/-}$ mice. Specifically, the loss of AMPARs from IHC afferent PSDs should result in a reduction in the strength of glutamatergic afferent signaling in Shank1$^{-/-}$ compared to Shank1$^{+/+}$ mice in response to auditory stimuli of equal intensities. Depending on the magnitude of reduction, an increase in ABR thresholds, decrease in P1–N1 amplitudes, and increase in P1 latencies specifically at lower frequencies would be predicted in Shank1$^{-/-}$ compared to Shank1$^{+/+}$ mice. To test this prediction, we recorded auditory brainstem responses (ABRs) from Shank1$^{+/+}$ and Shank1$^{-/-}$ littermate mice as described in the Methods (Fig. 5A). ABR thresholds were obtained at three frequencies: 8, 16, and 32 kHz. Although mean ABR thresholds were indeed elevated at 8 kHz in Shank1$^{-/-}$ mice (60 ± 7 dB peSPL) compared to Shank1$^{+/+}$ littermates (46 ± 3 dB peSPL), this difference was not statistically significant nor were differences in thresholds between genotypes at 16 and 32 kHz statistically significant. We also examined first peak amplitude (P1–N1) and latencies (P1). For both Shank1$^{+/+}$ and Shank1$^{-/-}$ littermate mice, as stimulus intensity increased, ABR amplitudes increased and latencies decreased (raw traces not shown). To compare changes across genotypes and frequencies, we calculated (as described in the Methods) input/output (I/O) linear regression slopes for amplitudes (Fig. 5B) and latencies (Fig. 5C) as a function of stimulus intensity at 3 frequencies (8, 16, and 32 kHz). There were no significant differences between genotypes for any of the tested frequencies. Raw values for ABR data are provided in Table 5. These findings indicate that changes in IHC afferent PSD composition, specifically the absence of Shank1 and concomitant reduction in AMPAR and GKAP expression, do not cause measurable auditory deficits in Shank1$^{-/-}$ compared to Shank1$^{+/+}$ littermates. Moreover, wave II amplitudes and latencies were quantified and compared between genotypes; however, no significant differences were observed. Although not quantified, waves III through V also showed no striking differences across genotypes. These data suggest that the absence of Shank1 does not disrupt synapse further along the auditory pathway. Although there were no effects of genotype on ABR thresholds, thresholds were elevated in both genotypes compared to CBA mice (Mock et al., 2011), suggesting mild hearing loss in both genotypes. This observation is consistent with a mild early onset hearing loss reported for the 129 mouse strain (Zheng et al., 1999), the background strain of these mice. Finally, we also observed intact DPOAEs in both genotypes, excluding substantial functional pathology of the OHCs in Shank1$^{-/-}$ mice and consistent with the observed absence of Shank1 in the OHC afferent PSDs.

3.4. Vestibular function is normal in the absence of Shank1

For completeness, we also examined the expression of Shank1 in the vestibular sensory epithelia using immunofluorescence and vestibular function of Shank1$^{-/-}$ mice. Vestibular afferent neurotransmission also relies on glutamatergic signaling (recently reviewed in Eatock and Songer, 2011). We triple immunolabeled isolated vestibular sensory epithelia of the utricular macula from Shank1$^{+/+}$ and Shank1$^{-/-}$ littermate mice with the mouse polyclonal antibody against Shank1 (red, Fig. 6A,E), the mouse monoclonal antibody against PSD95 (green, Fig. 6B,F), and a mouse monoclonal IgG1 antibody that recognizes tubulin J, a neurofilament enriched in the afferent calyx and bouton terminals (TuJ, blue, Fig. 6C,G; Perry et al., 2003). For these experiments, images of the striolar region were examined. We observed Shank1 immunoreactivity in the vestibular sensory epithelia isolated from Shank1$^{+/+}$ but not Shank1$^{-/-}$ mice, indicating that Shank1 is also normally expressed in the vestibular sensory epithelia. In Shank1$^{+/+}$ mice, Shank1 immunoreactivity was almost always colocalized with PSD95-positive PSDs (Fig. 6C,D) associated with both calyx and bouton vestibular afferent terminals, indicating that Shank1 is, not surprisingly, part of the vestibular afferent PSD. In Shank1$^{-/-}$ mice, we also observed PSD95-positive PSDs associated with both types of afferent terminals (Fig. 6G,H). Across

Table 4
IHC afferent PSD immunopuncta volumes.

	8 kHz				32 kHz			
	GluA2/3		GKAP		GluA2/3		GKAP	
	Shank1$^{+/+}$ (n = 4)	Shank1$^{-/-}$ (n = 7)	Shank1$^{+/+}$ (n = 4)	Shank1$^{-/-}$ (n = 7)	Shank1$^{+/+}$ (n = 4)	Shank1$^{-/-}$ (n = 7)	Shank1$^{+/+}$ (n = 4)	Shank1$^{-/-}$ (n = 7)
Mean ± SEM	1.78 ± 0.06	1.33 ± 0.74	1.53 ± 0.05	1.16 ± 0.03	1.52 ± 0.04	1.51 ± 0.03	1.28 ± 0.04	1.21 ± 0.03
N (immunopuncta)	799	1586	852	1.659	910	1625	1073	1622

Table 5
ABR values.

Frequency (kHz)	Thresholds (dB peSPL)		P1–N1 amplitude I/O slopes (μV/dB)		P1 Latency I/O slopes (-μs/dB)	
	Shank1$^{+/+}$ (n = 4)	Shank1$^{-/-}$ (n = 5–7)	Shank1$^{+/+}$ (n = 4)	Shank1$^{-/-}$ (n = 5–7)	Shank1$^{+/+}$ (n = 4)	Shank1$^{-/-}$ (n = 5–7)
8	46 ± 3	60 ± 7	0.027 ± 0.004	0.026 ± 0.004	16.0 ± 1.0	13.8 ± 0.9
16	38 ± 12	35 ± 8	0.045 ± 0.004	0.035 ± 0.004	11.3 ± 5.5	14.4 ± 2.9
32	44 ± 5	51 ± 8	0.031 ± 0.003	0.024 ± 0.004	12.7 ± 4.1	21.0 ± 6.3

samples, PSD95-positive PSDs appeared smaller (mirroring the trend observed in the organs of Corti of Shank1$^{-/-}$ mice) and less abundant in Shank1$^{-/-}$ compared to Shank1$^{+/+}$ mice. Analysis of PSD95-positive PSD areas from individual optical sections using methodology described previously (Pyott et al., 2004) indicated that PSD95-positive PSDs were not smaller although they were less numerous (approximately 30% less PSD95-positive PSDs per μm^2) in Shank1$^{-/-}$ compared to Shank1$^{+/+}$ mice. Further quantification of 3D reconstructions would be necessary to corroborate this finding and identify the types of afferent PSDs (bouton or calyx) that are potentially sparser in Shank1$^{-/-}$ mice. Although not quantified, GluA2/3-positive PSDs were also observed in the vestibular sensory epithelia of both Shank1$^{+/+}$ and Shank1$^{-/-}$ mice (data not shown). Functionally, as observed for ABRs, we found no differences in vestibular sensory evoked responses (VsEPs) between Shank1$^{+/+}$ and Shank1$^{-/-}$ littermates. There were no significant differences in thresholds (Shank1$^{+/+}$: -8.3 ± 0.8 dB re: 1.0 g/ms, n = 4; Shank1$^{-/-}$: −9.9 ± 1.1 dB re: 1.0 g/ms, n = 5; Fig. 6B) or P1–N1 amplitude I/O slopes (Shank1$^{+/+}$: 0.020 ± 0.007 μV/dB, n = 4; Shank1$^{-/-}$: 0.020 ± 0.010 μV/dB, n = 5; Fig. 6J). Although there was a trend of flatter P1 latency I/O slopes in Shank1$^{-/-}$ compared to Shank1$^{+/+}$ mice, this trend was not significant (Shank1$^{+/+}$: 0.036 ± 0.011 ms/dB, n = 4; Shank1$^{-/-}$: 0.020 ± 0.003 ms/dB, n = 5; Fig. 6K).

4. Discussion

Analogous to glutamatergic synapses in the CNS, afferent synapses of the inner ear likely shape their response properties via the molecular composition of their PSDs. Of the multitude of proteins comprising the PSD proteins, Shank proteins (1–3) are considered the “master” molecular determinants of the PSD composition, with the loss of Shank proteins associated with altered protein composition of the PSD and weaker glutamatergic signaling (Hung et al., 2008; Peca et al., 2011; Schmeisser et al., 2012) in the CNS. Motivated by these findings, we investigated the morphological and functional contribution of Shank proteins to the glutamatergic afferent synapses of the inner ear and especially cochlea. In summary, by immunofluorescence, we verified the expression of Shank1 in the IHC afferent PSDs (Figs. 1 and 2). We found no evidence by immunofluorescence for the expression of Shank2 and Shank3, the two other known Shank isoforms, in the afferent synapses (Fig. 2). These findings were corroborated by qPCR, in which we detected abundant *Shank1* transcript and very little *Shank2* and *Shank3* transcript in the organs of Corti and spiral ganglion cells (Fig. 2). We then investigated the morphology, composition, and function of IHC afferent PSDs in the cochlea of Shank1$^{-/-}$ mouse, which presumably lack all three Shank isoforms (see Fig. 2G). Although we found subtle changes in the morphology and composition (but not number and localization) of IHC afferent PSDs, specifically a reduction in size and GluA2/3 and GKAP expression at the lower frequency region (8 kHz) in Shank1$^{-/-}$ mice (Fig. 4), we detected no differences in ABRs compared to Shank1$^{+/+}$ littermate mice (Fig. 5). We also identified Shank1 in the vestibular afferent synapses, but detected no differences in VsEPs in Shank1$^{-/-}$ compared to Shank1$^{+/+}$ littermate mice (Fig. 6).

Given the enormous importance of Shank proteins to the composition, form, and strength of glutamatergic synapses in the CNS, these results are very surprising and lead to a variety of interpretations. First, our data show, at the very least, that Shank1 plays little role organizing IHC afferent PSDs, either during their prehearing establishment or maintenance after the onset of hearing. These results were unexpected considering that, in the CNS, even single genetic deletions of Shank proteins (Hung et al., 2008; Peca et al., 2011; Schmeisser et al., 2012) result in a range of ultrastructural, molecular, physiological and behavioral deficits, leading to the conclusion that there is, at most, only partial redundancy and functional compensation across isoforms. On the other hand, a diminished role of Shank1 in the inner ear compared to the CNS may reconcile the conspicuous absence of Shank1 in the outer hair cell (type II) afferent synapses that we and others (Huang et al., 2012) observed. Outer hair cell afferent synapse are also glutamatergic (Weisz et al., 2009) and presumably organize their PSDs with a set of proteins similar to those found in IHC afferent synapses and glutamateric synapses of the CNS but, as this work suggests, without the requirement of Shank1.

Second, our data indicate that Shank2 and Shank3 are not expressed in the mouse cochlea after the onset of hearing. Importantly, failure to detect a protein or transcript cannot be considered proof of its absence and further experiments will be needed to confirm the absence of Shank2 and Shank3 in the cochlea. With this caveat in mind, it is at least plausible that Shank1 is the only isoform expressed in the mouse cochlea. Non-overlapping distributions of Shank isoforms have been reported in the CNS: for example, Shank2 and Shank3 show complementary distribution in the cerebellum, with Shank2 mRNA expressed only in Purkinje cells and Shank3 mRNA expressed only in granule cells (Boeckers et al., 1999). If Shank1 is indeed the only Shank isoform expressed in the mouse cochlea, then our findings would further suggest that Shank1, 2, and 3 play little role organizing afferent PSDs in the cochlea. Importantly, our data do not exclude the possibility that Shank2 and 3 are expressed transiently before the onset of hearing and may contribute to the maturation of inner hair cell afferent synapses and potentially compensate for the loss of Shank1. Transient, prehearing expression has been observed for synaptotagmin proteins (Syt1 and Syt2) and suggests that the molecular composition of immature inner hair cell synapses may, in fact, be more similar to central synapses than synapses from mature inner hair cells (Beurg et al., 2010). To test the possible contributions of Shank2 and 3 to afferent synapse development and function explicitly, the auditory function of Shank2$^{-/-}$ and Shank3$^{-/-}$ as well as double and triple knockouts (if they are viable) should be investigated.

Third, if Shank proteins are nonetheless necessary components of IHC afferent PSDs in the cochlea and Shank1, 2, and 3 play little role organizing afferent PSDs in the cochlea, then our data suggest the possibility that other Shank isoforms, specific to the inner ear, exist. Although the pan-Shank antibody failed to detect protein in organs of Corti from Shank1$^{-/-}$ mice, the existence of inner ear specific isoforms is, nevertheless, not without precedent. In fact, a handful of proteins necessary for glutamateric signaling that are relatively selectively expressed in the

inner ear have been identified. For example, VGLUT3, a vesicular glutamate transporter (Seal et al., 2008), otoferlin, a Ca^{2+} sensor necessary for glutamate release from hair cells (Roux et al., 2006), and EAAT5, a glutamate transporter expressed in the vestibular sensory epithelia (Dalet et al., 2012) show more or less restricted expression to the inner ear (or ribbon synapses). Therefore, future work should investigate the expression of novel Shank isoforms in the inner ear.

Fourth, we cannot exclude the possibility that a change in form or function of inner ear afferent PSDs in Shank1$^{-/-}$ mice was not inadvertently overlooked. The PSD is comprised of a vast number of proteins, of which we only examined for differences in a subset of the receptor types mediating afferent synaptic transmission, GluA2/3, and a direct binding partner of Shank, GKAP. However, the minimal changes in PSD composition observed in the cochleae from Shank1$^{-/-}$ mice compared to Shank1$^{+/+}$ littermates failed to motivate a more exhaustive examination. Similarly, as discussed in the Results, auditory function was measured on a background strain known to show elevated hearing thresholds (Zheng et al., 1999) that were also observed in our examination. Nonetheless, profound hearing loss was not observed in Shank1$^{-/-}$ mice and thresholds, P1–N1 amplitude I/O slopes, and P1 latency I/O slopes were not statistically significantly different between Shank1$^{-/-}$ mice and Shank1$^{+/+}$ littermates. The lack of significant findings in these animals did not justify an effort to backcross this mouse onto a strain that does not show accelerated age-related hearing loss. Finally, Shank proteins are also known regulators of NMDAR and mGluR expression (Sheng and Kim, 2000). Very little is known about the functional contributions of these two receptor families to mammalian inner ear synaptic transmission (but see Kleinlogel et al., 1999; Doleviczenyi et al., 2005; Ruel et al., 2007), so potential differences in NMDAR or mGluR signaling in the inner due to the loss of Shank1 was not investigated but could nonetheless prove insightful.

In conclusion, our findings contribute to the growing body of work that emphasizes that, while there are many conserved molecular players between CNS and inner ear glutamatergic synapses, there are also differences that almost certainly underlie their functional differences. Importantly, even mature glutamatergic synapses of the CNS display remarkable plasticity over varying timescales, and Shank proteins appear to be important for that plasticity (recently reviewed in Zheng et al., 2011). Although reversible changes in surface AMPAR expression following acoustic overexposure have been shown *in vivo* (Chen et al., 2007), under normal conditions glutamatergic synapses of the inner ear may, by necessity, be much less plastic than their CNS counterparts and, therefore, have different demands of their repertoire of PSD scaffolding proteins.

Acknowledgments

We thank Ryan Byrns and Isabel Campos (University of North Carolina Wilmington) with assistance analyzing immunopuncta volumes. This work was supported by funds from the University of North Carolina Wilmington (S. J. P.), the Nebraska Tobacco Settlement Biomedical Research Foundation (S. V. and T. A. J.) and the Department of Special Education and Communication Disorders, University of Nebraska Lincoln (T. A. J. and S. M. J.). Various monoclonal antibodies used in this research were developed by and/or obtained from the UC Davis/NIH NeuroMab Facility, supported by NIH grant U24NS050606 and maintained by the Department of Neurobiology, Physiology and Behavior, College of Biological Sciences, University of California, Davis, CA 95616.

References

Beurg, M., Michalski, N., Safieddine, S., Bouleau, Y., Schneggenburger, R., Chapman, E.R., Petit, C., Dulon, D., 2010. Control of exocytosis by synaptotagmins and otoferlin in auditory hair cells. J. Neurosci. 30, 13281–13290.
Boeckers, T.M., Winter, C., Smalla, K.H., Kreutz, M.R., Bockmann, J., Seidenbecher, C., Garner, C.C., Gundelfinger, E.D., 1999. Proline-rich synapse-associated proteins ProSAP1 and ProSAP2 interact with synaptic proteins of the SAPAP/GKAP family. Biochem. Biophys. Res. Commun. 264, 247–252.
Boeckers, T.M., Segger-Junius, M., Iglauer, P., Bockmann, J., Gundelfinger, E.D., Kreutz, M.R., Richter, D., Kindler, S., Kreienkamp, H.J., 2004. Differential expression and dendritic transcript localization of Shank family members: identification of a dendritic targeting element in the 3' untranslated region of Shank1 mRNA. Mol. Cell. Neurosci. 26, 182–190.
Burkard, R., Feldman, M., Voigt, H.F., 1990. Brainstem auditory-evoked response in the rat. Normative studies, with observations concerning the effects of ossicular disruption. Audiology 29, 146–162.
Chen, Z., Kujawa, S.G., Sewell, W.F., 2007. Auditory sensitivity regulation via rapid changes in expression of surface AMPA receptors. Nat. Neurosci. 10, 1238–1240.
Dalet, A., Bonsacquet, J., Gaboyard-Niay, S., Calin-Jageman, I., Chidavaenzi, R.L., Venteo, S., Desmadryl, G., Goldberg, J.M., Lysakowski, A., Chabbert, C., 2012. Glutamate transporters EAAT4 and EAAT5 are expressed in vestibular hair cells and calyx endings. PLoS One 7, e46261.
Davies, C., Tingley, D., Kachar, B., Wenthold, R.J., Petralia, R.S., 2001. Distribution of members of the PSD-95 family of MAGUK proteins at the synaptic region of inner and outer hair cells of the guinea pig cochlea. Synapse 40, 258–268.
Doleviczenyi, Z., Halmos, G., Repassy, G., Vizi, E.S., Zelles, T., Lendvai, B., 2005. Cochlear dopamine release is modulated by group II metabotropic glutamate receptors via GABAergic neurotransmission. Neurosci. Lett. 385, 93–98.
Eatock, R.A., Songer, J.E., 2011. Vestibular hair cells and afferents: two channels for head motion signals. Annu. Rev. Neurosci. 34, 501–534.
el Barbary, A., 1991. Auditory nerve of the normal and jaundiced rat. I. Spontaneous discharge rate and cochlear nerve histology. Hear Res. 54, 75–90.
Glowatzki, E., Fuchs, P.A., 2002. Transmitter release at the hair cell ribbon synapse. Nat. Neurosci. 5, 147–154.
Huang, L.C., Barclay, M., Lee, K., Peter, S., Housley, G.D., Thorne, P.R., Montgomery, J.M., 2012. Synaptic profiles during neurite extension, refinement and retraction in the developing cochlea. Neural Dev. 7, 38.
Hung, A.Y., Futai, K., Sala, C., Valtschanoff, J.G., Ryu, J., Woodworth, M.A., Kidd, F.L., Sung, C.C., Miyakawa, T., Bear, M.F., Weinberg, R.J., Sheng, M., 2008. Smaller dendritic spines, weaker synaptic transmission, but enhanced spatial learning in mice lacking Shank1. J. Neurosci. 28, 1697–1708.
Jones, S.M., Erway, L.C., Bergstrom, R.A., Schimenti, J.C., Jones, T.A., 1999. Vestibular responses to linear acceleration are absent in otoconia-deficient C57BL/6JEi-het mice. Hear Res. 135, 56–60.
Jones, S.M., Erway, L.C., Johnson, K.R., Yu, H., Jones, T.A., 2004. Gravity receptor function in mice with graded otoconial deficiencies. Hear Res. 191, 34–40.
Jones, T.A., Jones, S.M., 1999. Short latency compound action potentials from mammalian gravity receptor organs. Hear Res. 136, 75–85.
Khimich, D., Nouvian, R., Pujol, R., Tom Dieck, S., Egner, A., Gundelfinger, E.D., Moser, T., 2005. Hair cell synaptic ribbons are essential for synchronous auditory signalling. Nature 434, 889–894.
Kleinlogel, S., Oestreicher, E., Arnold, T., Ehrenberger, K., Felix, D., 1999. Metabotropic glutamate receptors group I are involved in cochlear neurotransmission. Neuroreport 10, 1879–1882.
Kuriyama, H., Jenkins, O., Altschuler, R.A., 1994. Immunocytochemical localization of AMPA selective glutamate receptor subunits in the rat cochlea. Hear Res. 80, 233–240.
Larionov, A., Krause, A., Miller, W., 2005. A standard curve based method for relative real time PCR data processing. BMC Bioinforma. 6, 62.
Liberman, L.D., Wang, H., Liberman, M.C., 2011. Opposing gradients of ribbon size and AMPA receptor expression underlie sensitivity differences among cochlear-nerve/hair-cell synapses. J. Neurosci. 31, 801–808.
Liberman, M.C., 1982. Single-neuron labeling in the cat auditory nerve. Science 216, 1239–1241.
Luo, L., Brumm, D., Ryan, A.F., 1995. Distribution of non-NMDA glutamate receptor mRNAs in the developing rat cochlea. J. Comp. Neurol. 361, 372–382.
Maison, S.F., Pyott, S.J., Meredith, A.L., Liberman, M.C., 2013. Olivocochlear suppression of outer hair cells in vivo: evidence for combined action of BK and SK2 channels throughout the cochlea. J. Neurophysiol. 109, 1525–1534.
Matsubara, A., Laake, J.H., Davanger, S., Usami, S., Ottersen, O.P., 1996. Organization of AMPA receptor subunits at a glutamate synapse: a quantitative immunogold analysis of hair cell synapses in the rat organ of Corti. J. Neurosci. 16, 4457–4467.
McLean, W.J., Smith, K.A., Glowatzki, E., Pyott, S.J., 2009. Distribution of the Na,K-ATPase alpha subunit in the rat spiral ganglion and organ of corti. J. Assoc. Res. Otolaryngol. 10, 37–49.
Meyer, A.C., Frank, T., Khimich, D., Hoch, G., Riedel, D., Chapochnikov, N.M., Yarin, Y.M., Harke, B., Hell, S.W., Egner, A., Moser, T., 2009. Tuning of synapse number, structure and function in the cochlea. Nat. Neurosci. 12, 444–453.
Mock, B., Jones, T.A., Jones, S.M., 2011. Gravity receptor aging in the CBA/CaJ strain: a comparison to auditory aging. J. Assoc. Res. Otolaryngol. 12, 173–183.
Mueller, M., von Hunerbein, K., Hoidis, S., Smolders, J.W., 2005. A physiological place-frequency map of the cochlea in the CBA/J mouse. Hear Res. 202, 63–73.

Nouvian, R., Beutner, D., Parsons, T.D., Moser, T., 2006. Structure and function of the hair cell ribbon synapse. J. Membr. Biol. 209, 153–165.
Peca, J., Feliciano, C., Ting, J.T., Wang, W., Wells, M.F., Venkatraman, T.N., Lascola, C.D., Fu, Z., Feng, G., 2011. Shank3 mutant mice display autistic-like behaviours and striatal dysfunction. Nature 472, 437–442.
Perry, B., Jensen-Smith, H.C., Luduena, R.F., Hallworth, R., 2003. Selective expression of beta tubulin isotypes in gerbil vestibular sensory epithelia and neurons. J. Assoc. Res. Otolaryngol. 4, 329–338.
Pyott, S.J., Glowatzki, E., Trimmer, J.S., Aldrich, R.W., 2004. Extrasynaptic localization of inactivating calcium-activated potassium channels in mouse inner hair cells. J. Neurosci. 24, 9469–9474.
Roux, I., Safieddine, S., Nouvian, R., Grati, M., Simmler, M.C., Bahloul, A., Perfettini, I., Le Gall, M., Rostaing, P., Hamard, G., Triller, A., Avan, P., Moser, T., Petit, C., 2006. Otoferlin, defective in a human deafness form, is essential for exocytosis at the auditory ribbon synapse. Cell 127, 277–289.
Ruel, J., Wang, J., Rebillard, G., Eybalin, M., Lloyd, R., Pujol, R., Puel, J.L., 2007. Physiology, pharmacology and plasticity at the inner hair cell synaptic complex. Hear Res. 227, 19–27.
Safieddine, S., El-Amraoui, A., Petit, C., 2012. The auditory hair cell ribbon synapse: from assembly to function. Annu. Rev. Neurosci. 35, 509–528.
Sager, C., Tapken, D., Kott, S., Hollmann, M., 2009. Functional modulation of AMPA receptors by transmembrane AMPA receptor regulatory proteins. Neuroscience 158, 45–54.
Sala, C., Piech, V., Wilson, N.R., Passafaro, M., Liu, G., Sheng, M., 2001. Regulation of dendritic spine morphology and synaptic function by Shank and Homer. Neuron 31, 115–130.
Schmeisser, M.J., et al., 2012. Autistic-like behaviours and hyperactivity in mice lacking ProSAP1/Shank2. Nature 486, 256.
Schuth, O., McLean, W.J., Eatock, R.A., Pyott, S.J., 2014. Distribution of Na,K-ATPase alpha subunits in rat vestibular sensory epithelia. J. Assoc. Res. Otolaryngol. 15, 739–754.
Seal, R.P., Akil, O., Yi, E., Weber, C.M., Grant, L., Yoo, J., Clause, A., Kandler, K., Noebels, J.L., Glowatzki, E., Lustig, L.R., Edwards, R.H., 2008. Sensorineural deafness and seizures in mice lacking vesicular glutamate transporter 3. Neuron 57, 263–275.
Sheng, M., Kim, E., 2000. The Shank family of scaffold proteins. J. Cell. Sci. 113 (Pt 11), 1851–1856.
Sheng, M., Hoogenraad, C.C., 2007. The postsynaptic architecture of excitatory synapses: a more quantitative view. Annu. Rev. Biochem. 76, 823–847.
Silverman, J.L., Turner, S.M., Barkan, C.L., Tolu, S.S., Saxena, R., Hung, A.Y., Sheng, M., Crawley, J.N., 2011. Sociability and motor functions in Shank1 mutant mice. Brain Res. 1380, 120–137.
Taberner, A.M., Liberman, M.C., 2005. Response properties of single auditory nerve fibers in the mouse. J. Neurophysiol. 93, 557–569.
Truett, G.E., Heeger, P., Mynatt, R.L., Truett, A.A., Walker, J.A., Warman, M.L., 2000. Preparation of PCR-quality mouse genomic DNA with hot sodium hydroxide and tris (HotSHOT). Biotechniques 29 (52), 54.
Tsuji, J., Liberman, M.C., 1997. Intracellular labeling of auditory nerve fibers in guinea pig: central and peripheral projections. J. Comp. Neurol. 381, 188–202.
Vincent, P.F., Bouleau, Y., Safieddine, S., Petit, C., Dulon, D., 2014. Exocytotic machineries of vestibular type I and cochlear ribbon synapses display similar intrinsic otoferlin-dependent Ca^{2+} sensitivity but a different coupling to Ca^{2+} channels. J. Neurosci. 34, 10853–10869.
Weisz, C., Glowatzki, E., Fuchs, P., 2009. The postsynaptic function of type II cochlear afferents. Nature 461, 1126–1129.
Wersinger, E., McLean, W.J., Fuchs, P.A., Pyott, S.J., 2010. BK channels mediate cholinergic inhibition of high frequency cochlear hair cells. PLoS One 5, e13836.
Zheng, C.Y., Seabold, G.K., Horak, M., Petralia, R.S., 2011. MAGUKs, synaptic development, and synaptic plasticity. Neuroscientist 17, 493–512.
Zheng, Q.Y., Johnson, K.R., Erway, L.C., 1999. Assessment of hearing in 80 inbred strains of mice by ABR threshold analyses. Hear Res. 130, 94–107.